fire

MDPI

Article

Spatial Susceptibility Modeling and Driver Interpretation of Fire Occurrence in Southwest China

Jiaqi Liu [1], Fan Deng [1,*], Hui Li [2,*], Yinmei Zeng [1], Xiaopeng Guo [1] and Jiajia Guo [1]

[1] School of Geosciences, Yangtze University, Wuhan 430100, China; 2023710533@yangtzeu.edu.cn (J.L.); 2023720564@yangtzeu.edu.cn (Y.Z.); 2024710580@yangtzeu.edu.cn (X.G.); 2024720534@yangtzeu.edu.cn (J.G.)
[2] School of Geographical Science and Tourism, Nanyang Normal University, Nanyang 473061, China
* Correspondence: dengfan@yangtzeu.edu.cn (F.D.); huilidili@nynu.edu.cn (H.L.)

Abstract

Fire occurrence in Southwest China is jointly shaped by meteorological conditions, topography, vegetation status, and human activities. To improve the interpretability and validation rigor of regional fire susceptibility assessment, this study developed a grid-day-based susceptibility assessment framework for Yunnan, Sichuan, Guizhou, and Chongqing using MODIS active-fire detections and multi-source environmental data from 2015 to 2024 at a 5 km grid resolution. A sensitivity analysis was conducted to determine the training sample configuration, and a 1:2 positive-to-negative sampling ratio was adopted. Random Forest (RF), Support Vector Machine (SVM), and Logistic Regression (LR) were compared, and SHapley Additive exPlanations (SHAP), together with partial dependence plots (PDP), were used to interpret key drivers and their interactions. Data from 2015 to 2018 were used for model training, while data from 2019 to 2024 were used to evaluate the model's cross-year transferability within the same study domain, rather than full spatiotemporal independence. The results show that the 1:2 sampling ratio achieved a favorable balance between fire detection and false-alarm control. In five-fold stratified cross-validation, RF outperformed LR and SVM (AUC = 0.9167; F1-score = 76.70%). In the cross-year transferability test, areas classified as high and very high susceptibility captured 62.04–68.95% of the observed fire points while accounting for less than 32% of the total area. Soil moisture and maximum temperature contributed most strongly to the model output, and their interaction revealed a pronounced dry-hot statistical response pattern associated with elevated susceptibility. Fire susceptibility also exhibited stable positive spatial autocorrelation, with hotspot areas concentrated in the dry-hot valleys near the Sichuan-Yunnan border and in central-southern Yunnan. Because the model was built with under-sampled negatives and same-day environmental matching, the output should be interpreted as a relative fire susceptibility index for spatial assessment and statistical attribution rather than as a calibrated occurrence probability or a forward-looking daily forecast.

Keywords: fire susceptibility assessment; random forest; explainable machine learning; imbalanced sampling; spatial autocorrelation; Southwest China

Check for updates

Academic Editor: Grant Williamson

Received: 2 June 2026
Revised: 25 June 2026
Accepted: 3 July 2026
Published: 5 July 2026

Copyright: © 2026 by the authors. Licensee MDPI, Basel, Switzerland. This article is an open access article distributed under the terms and conditions of the Creative Commons Attribution (CC BY) license.

1. Introduction

Fire is a destructive global phenomenon driven by the interplay of climatic, topographic, vegetative, and anthropogenic factors [1]. Fire causes damage to surface vegetation and soil structures and releases harmful gases, thereby impairing atmospheric quality and ecosystem stability [2–4].

In the context of global warming, the frequent occurrence of extreme high-temperature and drought events has significantly increased the frequency and intensity of fires [5]. Southwest China (Yunnan, Guizhou, Sichuan, and Chongqing) features dramatic topographic relief, complex ecosystems, and abundant forest resources, making it one of the regions in China where fires occur frequently [6,7]. The region hosts a widespread distribution of fire-prone tree species—such as *Pinus yunnanensis* and *Eucalyptus*—rendering it highly susceptible to frequent and rapidly spreading fires. These fires result in severe casualties, the destruction of forest canopies and understory vegetation, the disruption of soil carbon and nitrogen cycles, biodiversity loss, and significant challenges for the long-term recovery of affected ecosystems [8]. Therefore, conducting fire susceptibility assessments and analyzing the influence of fire-driving factors is of great significance for mitigating regional disaster losses.

Methods for spatial assessment of fire susceptibility have evolved from traditional statistical models to machine learning (ML) approaches [9]. Early research predominantly utilized parametric models such as Logistic Regression (LR) [10]. With improvements in multi-source data and computational power, methods like Random Forest (RF) and Support Vector Machine (SVM) have been widely applied [11–14] to characterize complex non-linear relationships and multi-factor interactions. Although ML models have improved assessment accuracy, their internal decision-making processes lack interpretability, restricting in-depth understanding of the driver attribution [15]. For instance, in the typical dry-hot valley environments of Southwest China, a "dry-hot" coupling effect may exist between soil moisture and high temperature [16]. Furthermore, fire susceptibility inherently possesses profound spatial attributes, wherein areas of high susceptibility typically exhibit distinct clustered or dispersed spatial patterns. Traditional machine learning models often struggle to characterize the non-linear interactions of fire-driving factors or the spatial clustering of fire susceptibility. This limitation restricts the model's practical utility for both statistical interpretation and regional fire prevention strategies.

In addition to model interpretability, sample configuration strategies also significantly impact model performance [17]. Fire events exhibit marked spatial sparsity, leading to a severe imbalance between positive and negative samples. Existing studies mostly adopt random sampling or construct 1:1 balanced samples to meet model training requirements. While this can mitigate class bias, its applicability in macro-scale spatial assessments remains to be explored. Systematically analyzing the impact of different sample ratios on model performance and spatial identification results is crucial for enhancing the practical application value of the models in fire prevention management.

Focusing on Yunnan, Sichuan, Guizhou, and Chongqing, this study develops a regional fire susceptibility assessment framework using a unified 5 km grid system and multi-source environmental data from 2015 to 2024 [18]. Compared to existing studies in this region that primarily rely on traditional probability calibrations or macro-climatic analyses, this framework integrates a 'grid-day' dataset matching framework and introduces SHapley Additive exPlanations (SHAP) and Partial Dependence Plots (PDP) to enhance model interpretability and understand how fire-driving factors influence fire susceptibility. Furthermore, this study employs Global Moran's Index (Moran's I) and Local Indicators of Spatial Association (LISA) to analyze the spatial distribution and clustering patterns of fire susceptibility. The specific objectives are to: (1) determine an appropriate positive-to-negative sampling ratio through sensitivity analysis and compare RF, SVM, and LR for susceptibility discrimination; (2) interpret the statistical contributions and interaction patterns of key fire-driving factors using SHAP and PDP; and (3) characterize the spatial clustering patterns of fire susceptibility using Global Moran's I and Local Indicators of Spatial Association (LISA).

It should be emphasized that the framework is designed for susceptibility assessment and statistical attribution under observed environmental conditions, rather than for calibrated probability prediction or strict causal inference. In this study, fire susceptibility refers to a relative index representing the propensity for fire occurrence within a grid cell under observed environmental and anthropogenic conditions, rather than a calibrated probability of future ignition.

2. Study Area and Data

2.1. Overview of the Study Area

The research area selected for this study encompasses the four provinces and municipalities of Southwest China (Yunnan, Sichuan, Guizhou, and Chongqing), covering a total area of approximately 1.139 million square kilometers (92°21′ E–110°11′ E, 21°08′ N–34°19′ N). This region is situated in the transition zone from the first to the second step of China's topography, generally presenting a "high in the west, low in the east" elevation pattern. It is characterized by continuous mountains and basin plains with drastic elevation differences and complex, rugged terrain (Figure 1). Under the combined influence of complex topography and monsoon circulation, the regional fire conditions exhibit significant spatiotemporal variations [19]. The western and southern parts, influenced by both the subtropical monsoon climate and the plateau, experience a high incidence of fires during the dry winter and spring seasons due to low precipitation. Conversely, the eastern basins and hilly areas, affected by the summer subtropical high-pressure system, may experience persistent high temperatures and sparse rainfall, rendering them highly susceptible to fires [20,21].

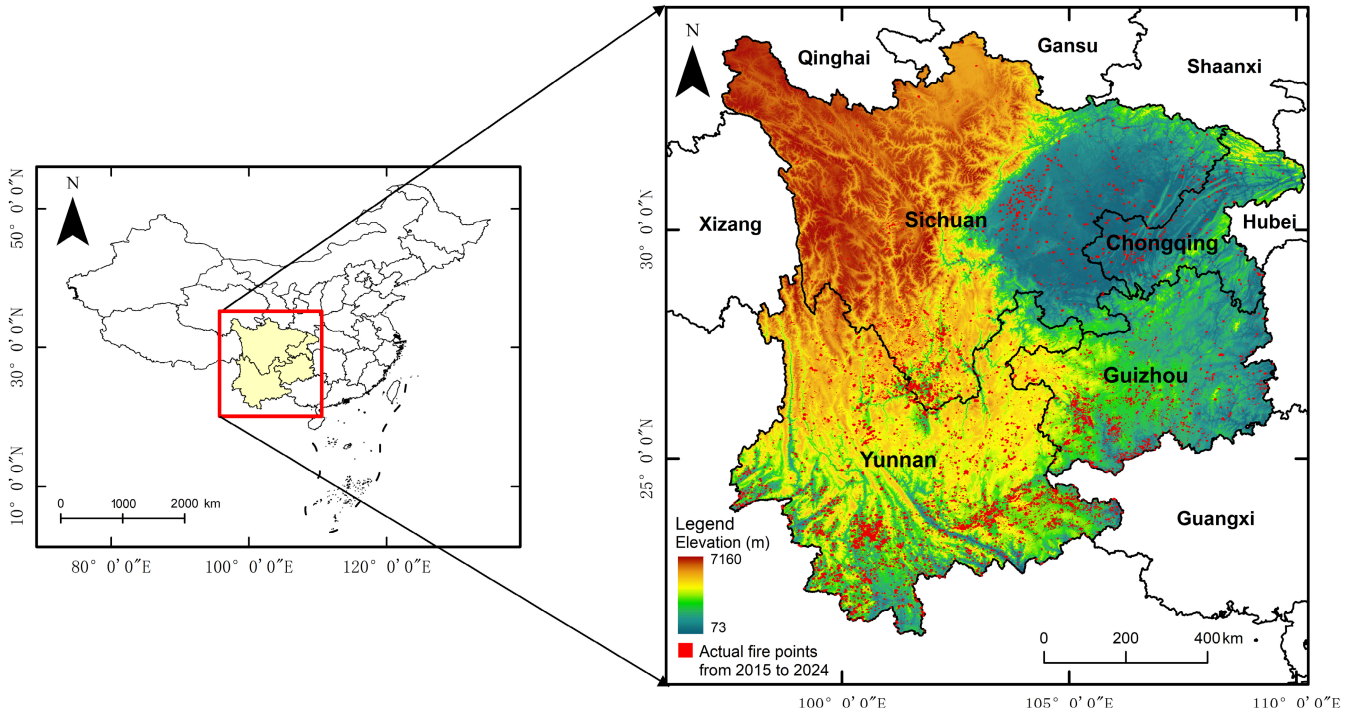


Figure 1. Location of the study area, its Digital Elevation Model (DEM), and the spatial distribution of actual fire points from 2015 to 2024.

Simultaneously, the study area is located in the southwestern forest region of China, widely covered with subtropical evergreen broad-leaved forests, warm temperate coniferous forests, and understory shrubs. Fallen branches and leaves form substantial litter

layers and fuel accumulations. Under drought conditions, the moisture content of this litter decreases significantly, providing potential fuel conditions for fires.

In summary, the complex topography, monsoon climate, and fuel conditions collectively form a fire-prone environment with highly heterogeneous fire triggers in the study area. Additionally, anthropogenic fire usage (such as agricultural burning and ritual activities) further increases fire susceptibility. Therefore, conducting macro-scale fire susceptibility assessment modeling and driving factor attribution analysis in this region possesses both practical applicability and research representativeness.

2.2. Data Sources and Preprocessing

This study constructed a long-time-series multi-source dataset covering the four provinces and municipalities of Southwest China from 2015 to 2024. It utilizes MODIS active fire data to generate data labels, combined with 12 environmental predictor variables, including remote sensing vegetation indices, meteorological reanalysis, and anthropogenic geographic information, to assess the relative susceptibility of fires.

2.2.1. Data Sources

The remote sensing and meteorological data for the study area were obtained from standardized advanced datasets published by institutions such as NASA and ECMWF on the Google Earth Engine (GEE) platform. The data underwent rigorous radiometric calibration, atmospheric correction, and precise geometric correction to generate standardized research datasets [22,23]. Anthropogenic impact factor data were sourced from the WorldPop global demographic research project initiated by the University of Southampton, and road vector data were obtained from the OpenStreetMap (OSM) open-source geographic information database.

The specific sources, spatial resolutions, and temporal resolutions of each dataset are detailed in Table 1.

Table 1. Details of the multi-source datasets used in this study.

Influencing Factors	Dataset (Product Version)	Spatial Resolution	Temporal Resolution
Fire Data	MOD14A1 Version 6.1	1 km	Daily
NDVI	MOD13A1 Version 6.1	500 m	16-day
Precipitation	CHIRPS v2.0 Daily	0.05°	Daily
Mean Temperature Maximum Temperature Wind Direction Soil Moisture	ERA5-Land hourly reanalysis	0.1°	Hourly
Elevation Slope Aspect	NASADEM HGT v1	30 m	Static
Land Cover Type	MCD12C1 Version 6.1	0.05°	Annual
Population Density	WorldPop Global Project	1 km	Year
Number of Roads Within the Grid	OpenStreetMap (OSM)	Vector	Static

2.2.2. Spatiotemporal Consistency Processing and Feature Encoding of Multi-Source Data

Multi-source heterogeneous data exhibit significant differences in original resolution and update frequency. This study used a 5 km × 5 km vector grid under the Albers Equal Area Conic projection as the spatial base and a daily temporal step to construct a unified "grid-day" spatiotemporal matching framework.

Dynamic meteorological variables were aggregated to the 5 km grid using the area-weighted average method and summarized at the daily scale. Variables derived from ERA5-Land, such as temperature and soil moisture, were used to represent regional-scale ambient hydrothermal conditions rather than localized instantaneous thermal anomalies. Nevertheless, because fire labels and environmental variables were matched on the same calendar day, this design cannot fully determine the sub-daily temporal ordering between fire occurrence and environmental conditions, nor can grid-scale aggregation eliminate potential same-day dependence. Therefore, these variables were used to characterize contemporaneous environmental backgrounds for susceptibility diagnosis. Restricted by its 16-day compositing interval, NDVI was aligned to a daily step using the Last Observation Carried Forward (LOCF) method, a conservative forward-filling strategy that propagates the most recent valid observation to subsequent missing time steps. Compared with linear interpolation, which reconstructs temporally smooth trajectories using both preceding and subsequent observations, the LOCF approach relies exclusively on historically available observations and avoids incorporating future information into current temporal estimates, thereby preserving temporal causality and reducing the risk of temporal look-ahead bias in predictive analyses [24]. Anthropogenic factors were directly calculated as spatial statistics within the grids and assigned fixed values.

For fire data, fire points were matched to the corresponding grids on the same day based on spatial joining. Through masking processing utilizing land cover data, fire points overlapping with water bodies and permanent snow/ice areas were excluded to filter out anomalous false detections. Urban and built-up areas were also removed to avoid false fire points generated by industrial thermal anomalies. The target of this study focuses on generalized fire susceptibility and total active-fire occurrence across the landscape, rather than categorizing the statistical records into specific sub-types. Therefore, after excluding anomalous thermal points in land cover types such as water bodies, various surface fires are retained to reflect broader regional fire dynamics. Valid grids with fires were marked as positive samples (value = 1), while remaining grids were extracted as negative samples (value = 0). For multi-class discrete variables like land cover types, One-Hot Encoding was applied to ensure fairness in feature distance measurement.

For circular variables such as aspect and wind direction, we employed a standardized trigonometric transformation $(Index = 1 - \cos\theta)$, which is a common practice in susceptibility modeling to address the circular discontinuity of azimuth data. By setting the direction of maximum solar exposure as the reference baseline, this transformation projects the circular azimuth values onto a continuous linear scale (0–2) [25]. This treatment effectively resolves the numerical distortions inherent in angular representations during statistical calculations (such as mean estimation). Methodologically, this approach serves as a parsimonious linearization simplification to capture general solar radiation contrasts, rather than a physically derived risk function.

Fire-driving variables operate across different temporal scales. Maximum temperature and precipitation represent concurrent meteorological conditions, whereas soil moisture and NDVI reflect antecedent environmental states. Rather than assuming a strict causal sequence, the machine-learning framework integrates these heterogeneous variables to characterize the combined environmental context associated with fire susceptibility. Accordingly, the model should be interpreted as a susceptibility assessment framework rather than a process-based fire forecasting model.

2.2.3. Construction of the Driving Factor System and Multicollinearity Diagnosis

The occurrence of fires is typically driven by multi-dimensional factors. Because varying degrees of correlation may exist among environmental variables, this study employed

the Variance Inflation Factor (VIF) to conduct a collinearity diagnosis on the driving factors. Its calculation formula is shown in Equation (1).

$$VIF_i = \frac{1}{1 - R_i^2} \quad (1)$$

where R_i^2 represents the coefficient of determination obtained when the i-th variable is used as the dependent variable and the remaining variables as independent variables in multiple linear regression.

To mitigate the influence of spatial autocorrelation, VIF diagnostics were computed using a sparse, randomized spatiotemporal sub-sample (10 million random samples) to minimize the impact of local spatial dependency on the VIF results. The diagnostic results (Table 2) reveal that among the 12 driving factors, the VIF values for mean temperature and maximum temperature reached 50.49 and 46.03, respectively, indicating extremely severe multicollinearity during the fire development process in Southwest China. Although non-linear ensemble models natively tolerate multicollinearity for predictive tasks, eliminating highly collinear variables effectively reduces data redundancy. More importantly, we employed VIF filtering as a deliberate structural choice to ensure the stability of the subsequent SHAP and PDP interpretability frameworks [26,27]. Maximum temperature was preferentially retained over mean temperature because extreme thermal conditions act as a more direct concurrent trigger for fuel moisture depletion and fire occurrence [28]. Following the exclusion of mean temperature, the VIF values of all remaining variables dropped below 5. It should be noted that VIF is primarily utilized to identify statistical collinearity and does not imply a strict causal interpretation.

Table 2. Variance Inflation Factor (VIF) of fire-driving factors before and after variable selection.

Variable	Initial VIF	Final VIF
Mean Temperature	50.49	—
Maximum Temperature	46.03	2.00
Precipitation	1.10	1.09
Wind Direction	1.14	1.11
Elevation	2.49	2.12
Slope	1.33	1.33
Aspect	1.00	1.00
NDVI	1.40	1.40
Soil Moisture	1.29	1.15
Road Density	2.20	2.20
Gridded Population Density	2.17	2.17
Land Cover Type	1.47	1.46

3. Methodology

3.1. Sample Construction

3.1.1. Definition of Positive and Negative Samples and Data Splitting

To construct a modeling dataset suitable for the large-scale study area, we implemented a "grid-day" spatiotemporal matching strategy. The 5 km × 5 km spatial grids were overlaid across the study area, and 10 years of daily records yielded approximately 192 million potential "grid-day" instances. If a MODIS active-fire point was detected in grid i on day t, that specific (grid i, day t) instance was labeled as a positive sample (value = 1), and its fire susceptibility driving factors were strictly extracted from the corresponding environmental datasets of day t. Conversely, if no fire was detected in grid j on day t', the instance was eligible to be included as a negative sample (value = 0), matching exactly with the contemporaneous fire susceptibility driving factors of day t'. This dynamic matching

ensures that the model learns to distinguish concurrent environmental conditions between fire days and non-fire days. Among the 192 million potential instances, the monitored active-fire records yielded a total of 42,643 positive samples. To train the model and conduct robust cross-year transferability validation, 15,525 positive samples from 2015 to 2018 were extracted to construct the model training set, while 27,118 positive samples from 2019 to 2024 were used to build an independent cross-year transferability validation set. Both sets were paired with their corresponding negative samples according to the optimal sampling ratio. Specifically, these negative samples were strictly extracted from non-fire grids on the exact same days as the positive fire events, thereby maintaining temporal consistency between the positive and negative samples and minimizing confounding effects arising from seasonal and interannual variability. This temporal division enables the model to be evaluated on completely unseen future data, thereby facilitating the examination of its cross-year transferability.

3.1.2. Sample Ratio Selection Based on Sensitivity Analysis

Fire occurrences are characterized by extreme sparsity in geographic space. Within the study region, the 10-year daily records across the spatial grids yielded approximately 192 million "grid-day" samples, among which the actual monitored active fire records generated only 42,643 positive samples, establishing an extremely imbalanced natural prior positive-to-negative sample ratio of approximately 1:4500. If a traditional global random under-sampling strategy were used to construct a strictly balanced 1:1 dataset, it would severely distort this highly imbalanced prior environment, forcing the models to systematically overestimate regional fire susceptibility and generate excessive false alarms in operational hazard mapping. To scientifically optimize the training environment, we designed a multi-model sensitivity analysis. While keeping the training positive samples constant, negative samples were extracted using random under-sampling at ratios incrementally increasing from 1:1 to 1:5 (with a step size of 0.5). This experiment was consistently evaluated across three machine learning frameworks (RF, SVM, and LR) to investigate the universal trade-off between theoretical classification metrics and practical false-alarm suppression.

As illustrated by the multi-model sensitivity performance (Figure 2), evaluation metrics such as the F1-score and AUC theoretically peaked at the 1:1 balanced ratio across all three algorithms. As the proportion of negative samples increased, the models' statistical criteria for classifying a potential fire source became stricter, leading to varying degrees of decline in the model metrics. While RF and SVM maintained relatively stable sensitivity at the 1:2 ratio, LR exhibited a rapid decline, with its recall dropping to 51.98%. In safety-relevant applications such as fire susceptibility assessment, missing nearly half of the actual occurrences represents a critical limitation. Given the inherent constraints of linear models in handling complex non-linear environmental interactions under imbalanced priors, accommodating this severe loss of recall in LR was not prioritized. Therefore, to capture a sufficiently large distribution of non-fire environmental conditions in the feature space without excessively degrading model sensitivity, we determined the 1:2 sampling ratio to be the optimal configuration, primarily based on the robust performance of RF and SVM [29,30]. Under this configuration, these non-linear models maintained relatively stable and balanced performance while successfully suppressing systematic spatial overestimation.

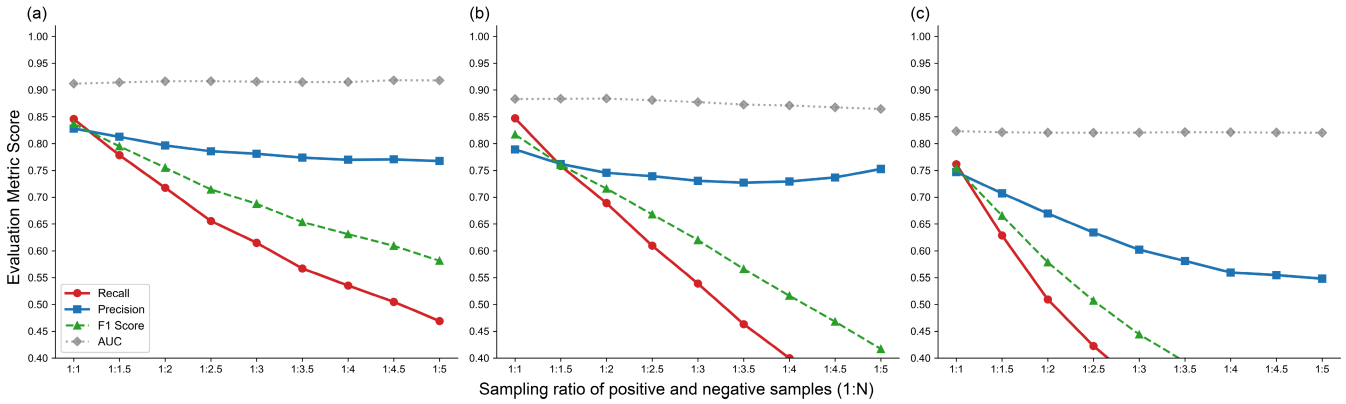


Figure 2. Changes in the classification performance of three machine learning models under different positive-to-negative sampling ratios: (**a**) RF; (**b**) SVM; (**c**) LR.

3.2. Machine Learning Models

3.2.1. Random Forest

The discrimination of fire occurrence is inherently a binary classification problem. However, given that negative samples were under-sampled during the training phase and the focus of this paper is on identifying the relative susceptibility background at a regional scale, the model output is interpreted herein as a "relative fire susceptibility index" rather than an absolute, calibrated occurrence probability. The continuous output ranging from 0 to 1 is therefore used for relative ranking and spatial comparison among grid cells. Because the fire driver attribution in Southwest China involves complex interactions among multi-dimensional factors—including meteorology, topography, and human activities—the RF algorithm was chosen to construct the fire susceptibility assessment model [31,32]. RF is an ensemble machine learning algorithm based on multiple decision trees. It exhibits excellent performance in handling high-dimensional data and complex non-linear relationships, while also showing strong robustness to outliers and data noise [33–35].

3.2.2. Baseline Comparative Models: LR and SVM

To comprehensively evaluate the performance of the RF model in assessing fire susceptibility in Southwest China, this study selected Logistic Regression (LR) and Support Vector Machine (SVM) as baseline comparative models.

LR is a classic binary classification algorithm based on the framework of generalized linear models. It utilizes the Logistic function to map linear combinations of multiple driving factors to the 0–1 interval, characterizing fire occurrence propensity. The LR model boasts high computational efficiency and intuitive parameter interpretability, thus serving as the performance benchmark for linear models in this study [36,37].

SVM is a supervised machine learning algorithm based on statistical learning theory. Its core concept is finding the optimal classification hyperplane in the feature space that maximizes the classification margin. When samples are non-linearly separable in their original space, kernel functions can map features to higher-dimensional spaces to construct non-linear classification boundaries. SVM possesses strong generalization capabilities in handling complex non-linear classification problems, earning its selection as the non-linear comparative model for this study [38,39].

By systematically comparing RF with linear (LR) and non-linear (SVM) models, the discriminative capabilities of different algorithms in identifying spatial variations in fire susceptibility under complex geographic conditions can be objectively assessed [40].

3.3. Model Evaluation Metrics

For the continuous output results of the models, this study introduced the Receiver Operating Characteristic (ROC) curve and its Area Under the Curve (AUC) to measure the overall discriminative capability of the models across different classification thresholds [41]. A multi-dimensional evaluation system based on the confusion matrix was employed to systematically quantify the classification accuracy and stability of RF and comparative models in fire susceptibility discrimination. Accuracy, Precision, Recall, and F1-score were selected as the core performance evaluation metrics [42]. Given that the model output is interpreted herein as a relative fire susceptibility index, these metrics are primarily used to compare the discriminative performance of different models rather than to evaluate the level of absolute probability calibration.

Model hyperparameters were tuned by grid search within the training data. To ensure computational reproducibility, the final RF model was configured with n_estimators = 200, max_depth = 25, min_samples_split = 4, and random_state = 42.

To comprehensively evaluate the models' discriminative performance and stability, this study implemented a two-stage validation strategy. For the 2015–2018 modeling dataset, stratified five-fold cross-validation was used only for an initial comparison of algorithmic discrimination performance [43]. Because random splitting may still retain spatiotemporal dependence among samples, these cross-validation metrics should not be interpreted as fully independent evidence of generalization. Therefore, data from 2019 to 2024 were further used for cross-year transferability tests within the same spatial domain to examine whether the spatial distribution patterns of fire susceptibility remained stable across years. The optimal model trained previously was applied for susceptibility mapping. The assessed high-susceptibility areas were spatially overlaid with the actual MOD14A1 fire points detected during the same period to calculate the fire point hit rate—a metric of greater operational significance. This process served to verify the model's robustness when confronted with unknown years.

3.4. SHAP-Based Driving Factor Attribution Analysis

The Random Forest algorithm relies on a complex architecture integrating multiple decision trees. Its internal decision-making process presents highly "black-box" characteristics, making it difficult to directly reveal the marginal contributions and interaction patterns of driving factors on fire susceptibility. To explain the internal decision logic of the model, this paper introduced the SHAP analysis framework, which is based on cooperative game theory [44,45].

By calculating the marginal contribution of each feature, the SHAP method expresses the output results of complex machine learning models as an additive decomposition of various influencing factors, thereby explaining the model's decision-making process. For any spatial grid sample x, the model output $f(x)$ can be expressed as the sum of the model's expected output and the SHAP values of each feature. The expression of its additive explanation model is shown in Equation (2).

$$f(x) = \phi_0 + \sum_{j=1}^{M} \phi_j \quad (2)$$

where $f(x)$ represents the model's output value for sample x; ϕ_0 is the expected value of the model output; M is the number of driving factors inputted into the model (after multicollinearity testing, this study retained $M = 11$ variables); and ϕ_j signifies the contribution value of the j-th feature to the model's output result. When $\phi_j > 0$, the variable exhibits a positive effect on fire occurrence; conversely, it has a negative effect.

3.5. Partial Dependence Plots and Multi-Factor Interaction Analysis

The SHAP framework focuses on local attribution at the discrete sample level. To further quantify the average response trends of core fire-driving factors to the model output across different value intervals, this paper introduced PDP. By marginalizing non-targeted features, PDP approximately depicts the average marginal effect of targeted features on the model's output results [46]. However, it should be clarified that the statistical response ranges identified in this study serve solely for statistical interpretation purposes and are not considered physical thresholds in a strict sense.

Suppose the input feature set is divided into a target feature subset X_s and the remaining feature subset X_c. The partial dependence function $\hat{f}_s(x_s)$ of the target feature is approximated using the empirical distribution of the training data, defined as Equation (3).

$$\hat{f}_s(x_s) = \frac{1}{N}\sum_{i=1}^{N} f(x_s, x_{ic}) \tag{3}$$

where N is the total number of samples; x_{ic} is the value of the i-th sample on the feature subset X_c. This study initially identified the non-linear statistical response ranges of key environmental factors based on univariate PDP curves and then further introduced two-dimensional partial dependence plots (2D-PDP). 2D-PDP can filter out the marginal interference of single variables and smooth the bivariate joint distribution into a continuous fire susceptibility response surface, thus analyzing the synergistic impacts under complex multi-factor coupling conditions.

The PDP method relies on the assumption of feature independence. In scenarios where features are highly correlated, the results may exhibit bias. Therefore, the patterns reflected by PDP under relevant environmental variables represent statistical response modes between features and model outputs. PDP should be regarded as an auxiliary explanation tool alongside SHAP, rather than being over-interpreted as direct causal inference. This study combined SHAP analysis results with PDP curves for cross-verification to enhance the robustness of the explanatory findings.

SHAP and PDP are used here to interpret the statistical response structure learned by the model. Their outputs should not be over-interpreted as direct evidence of causal mechanisms or universally transferable physical thresholds.

3.6. Spatial Autocorrelation Analysis

Natural environmental factors and human activities typically exhibit distance decay and local homogeneity characteristics in space. This study introduced the Global Moran's I and Local Indicators of Spatial Association (LISA) to conduct a spatial topological structure analysis of the relative fire susceptibility index output by the model [47]. This method is primarily used to quantify the macro-scale clustering patterns of the output results and identify the boundaries of cold and hot spots. It provides a qualitative reference from a geographical perspective for regional joint prevention and control, rather than serving as an independent validation metric for assessing model accuracy.

The calculation formula for the Global Moran's I index is shown as Equation (4).

$$I = \frac{n\sum_{i=1}^{n}\sum_{j=1}^{n} w_{ij}(x_i-\overline{x})(x_j-\overline{x})}{\left(\sum_{i=1}^{n}\sum_{j=1}^{n} w_{ij}\right)\sum_{i=1}^{n}(x_i-\overline{x})^2} \tag{4}$$

where n is the number of spatial units; x_i and x_j represent the fire susceptibility assessment values of grids i and j, respectively; $\overline{x}$ is the mean susceptibility value; w_{ij} is the element of the spatial weight matrix. This study employed the Queen first-order contiguity rule to define spatial adjacent relationships and performed calculations on the yearly average spatial

inference results of susceptibility. Statistical significance was evaluated by calculating the Z-score and *p*-value through a Monte Carlo permutation test.

4. Results

4.1. Comparative Evaluation of Model Classification Performance

Based on the modeling dataset from 2015 to 2018, this study employed stratified five-fold cross-validation to quantitatively assess the discriminative performance of three algorithms: LR, RF, and SVM. The results of this phase were primarily used to horizontally compare the fitting capabilities of different algorithms regarding fire susceptibility characteristics, facilitating the selection of the optimal modeling algorithm.

According to the ROC curves in Figure 3, the ROC curve for RF is positioned above those of the other two baseline models, with an AUC value of 0.9167, indicating a relatively higher discriminative performance on the available samples. However, it should be clarified that because fire samples exhibit strong continuity in both time and space, traditional random cross-validation may produce a certain degree of overestimation due to sample similarity. Consequently, this AUC score is strictly utilized to establish a relative performance comparison among the three baseline models. The framework's true generalization capacity and operational reliability are subsequently quantified by the spatial hit rate of actual fire occurrences falling within the designated susceptibility levels.

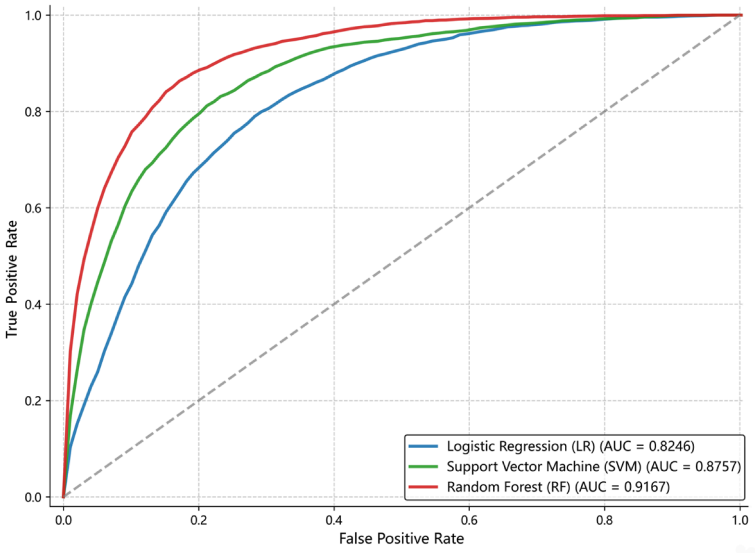


Figure 3. Comparison of ROC curves for three fire susceptibility assessment models.

Further analysis of various core evaluation metrics reveals statistical results as shown in Table 3. RF exhibited optimal comprehensive performance, achieving an accuracy of 85.01% and an F1-score of 76.70%, thereby realizing a sound balance between precision and recall.

Table 3. Comparison of comprehensive performance of different fire susceptibility assessment models.

Model	Accuracy	Precision	Recall	F1-Score	AUC Value
LR	75.77%	67.85%	51.98%	58.85%	0.8246
SVM	81.19%	74.77%	65.77%	69.98%	0.8757
RF	85.01%	79.61%	74.00%	76.70%	0.9167

Integrating the multi-dimensional evaluation metrics based on the confusion matrix and the AUC value from the ROC curves, RF was designated as the modeling algorithm

for the subsequent spatial deduction of fire susceptibility and in-depth deconstruction of key drivers in Southwest China.

4.2. Global Attribution Analysis of Fire Susceptibility Drivers

By calculating the marginal contribution of each feature under all feature combinations, the SHAP algorithm indicates the relative contributions of fire-driving factors within complex non-linear models. Compared to the limitations of traditional tree models, which evaluate feature importance solely based on metrics like Gini Impurity, SHAP realizes a ranking of feature importance and illustrates their positive or negative impacts on susceptibility results.

The global contribution ranking bar chart (Figure 4a) indicates that soil moisture, maximum temperature, elevation, and population density are the top four in importance. Soil moisture and maximum temperature occupy the first two spots, illustrating that fuel moisture status and thermal conditions contribute most significantly in statistical terms to the model output. As shown in Figure 4b, high values of soil moisture are concentrated in the negative SHAP interval, presenting a negative impact; high-temperature samples are predominantly distributed in the positive interval, presenting a positive impact; low-altitude areas contribute positively to fire susceptibility impacts, while high-altitude areas shift toward negative impacts; high-value samples of population density correspond to higher positive SHAP contributions, presenting a positive impact.

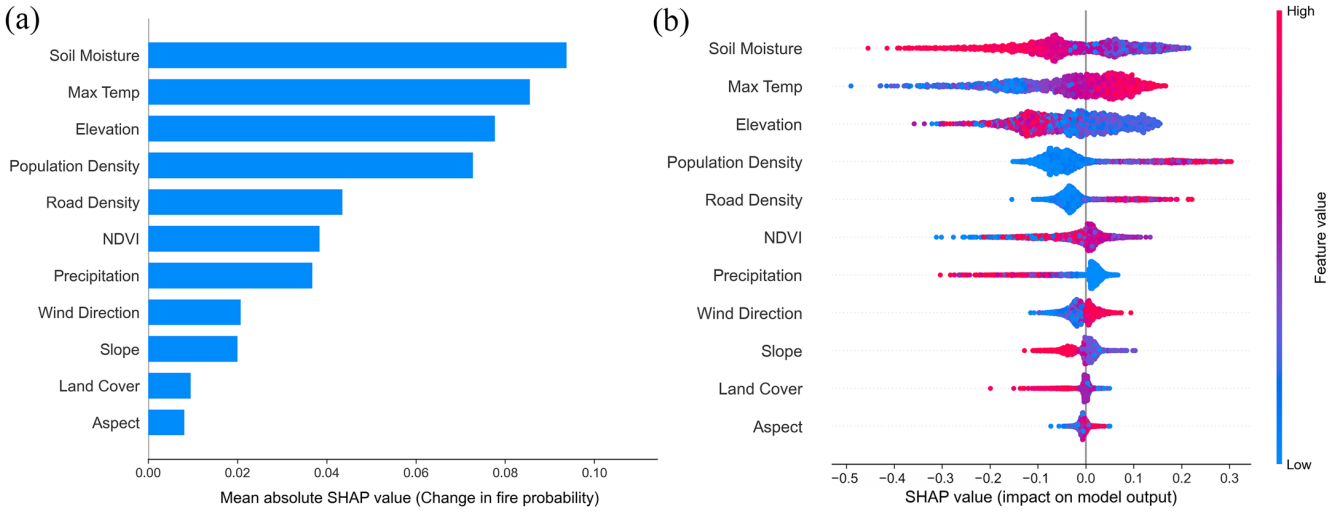


Figure 4. Global SHAP attribution analysis of fire susceptibility drivers in Southwest China (**a**) bar graph (**b**) beeswarm plot.

The significantly higher SHAP contributions of these four factors relative to the remaining variables indicate their relatively prominent positions within the model's explanatory framework and their considerable impact on the spatial distribution of fire susceptibility.

4.3. Fire Susceptibility Response Characteristics of Fire-Driving Factors

The global importance ranking bar chart and beeswarm plot ascertained the overall contribution differences and impact directions of individual factors; however, they cannot identify the specific driving trajectories of these variables across different intervals on the model output. Extracting the top four globally important factors—soil moisture, maximum temperature, elevation, and population density—partial dependence plots were drawn for these core impact factors (Figure 5) to further analyze their complex, non-linear influence variation laws.

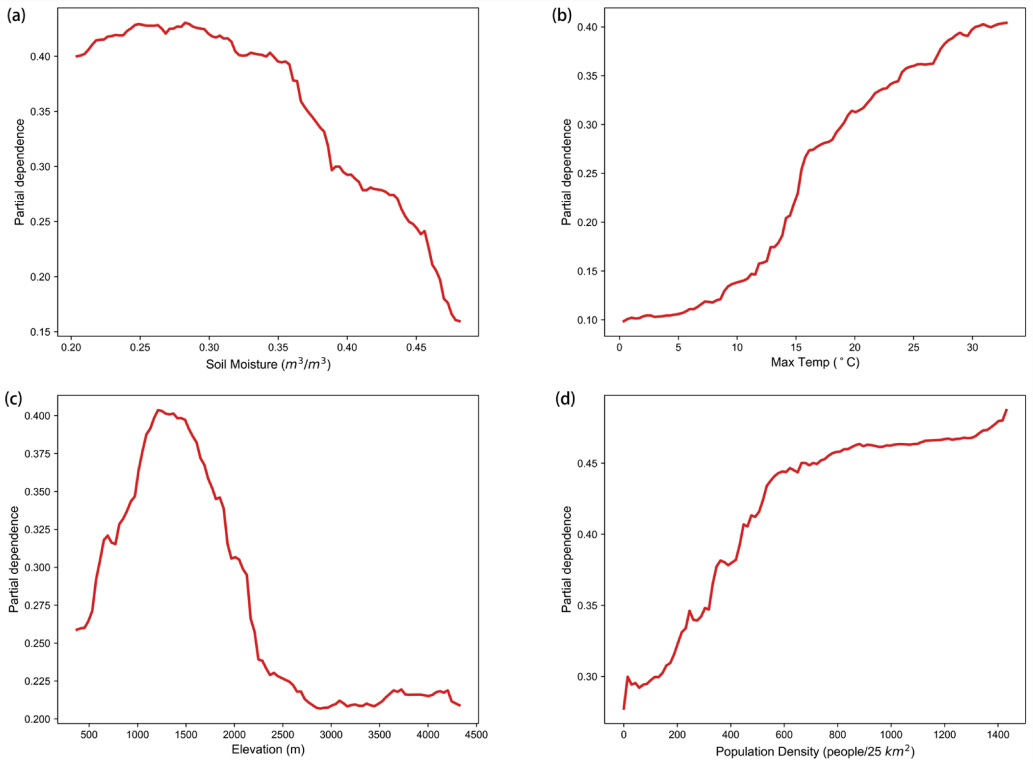


Figure 5. The local nonlinear response characteristics of fire susceptibility to the core driving factors (**a**) soil moisture; (**b**) maximum temperature; (**c**) elevation; (**d**) population density.

Soil moisture (Figure 5a) exhibited steep negative characteristics. When it was below approximately 0.35 m^3/m^3, fire susceptibility entered a high-susceptibility response range, indicating that surface drought serves as a distinct correlated background for heightened fire susceptibility. Upon breaching this response interval, susceptibility rapidly declined as moisture increased. This demonstrates that surface drought is the most significant fire-driving factor statistically associated with elevated fire susceptibility.

Maximum temperature (Figure 5b) displayed a phased upward trend. In lower numerical intervals under 20 °C, its positive association with fires was relatively faint, suggesting that meteorological conditions at this stage are insufficient to significantly promote conditions favorable for fire occurrence. Once maximum temperatures surpassed the potential statistical response range of 20 °C, the fire susceptibility curve showed a rapid increasing trend.

From an elevation perspective (Figure 5c), elevated susceptibility was primarily concentrated within the 800–2000 m interval, peaking prominently near 1500 m. When elevation exceeded 2500 m, susceptibility decreased sharply and stabilized at low levels.

At lower levels, population density (Figure 5d) displayed clear positive promotional effects, illustrating that human activities are positively correlated with higher susceptibility to fire source occurrences. However, in densely populated areas, the growth in susceptibility gradually flattened out due to changes in fire prevention and suppression management and land-use modalities [48].

The partial dependence plots of the above four driving factors illustrate that fire susceptibility possesses significant non-linear sensitivity toward key environmental factors and human activity variables, forming distinct statistical response ranges across specific intervals.

4.4. Interactive and Coupled Effects of Core Driving Factors

Fire occurrence is the result of the statistical interactions of extreme meteorology, topography, and human activities. This study further integrated SHAP feature dependence

plots and two-dimensional partial dependence plots to meticulously analyze the mutual impacts when these factors are superimposed.

As discernible from Figure 6, conditional dependencies exist among fire-driving factors in Southwest China. Taking the core moisture-heat combination of maximum temperature and soil moisture as an example, in Figure 6a,b, the correlation intensity between high temperature and susceptibility was perceptibly moderated by soil moisture. Under arid environments, escalating temperatures were significantly associated with higher relative fire susceptibility; conversely, in humid environments, the impacts induced by warming were substantially weakened.

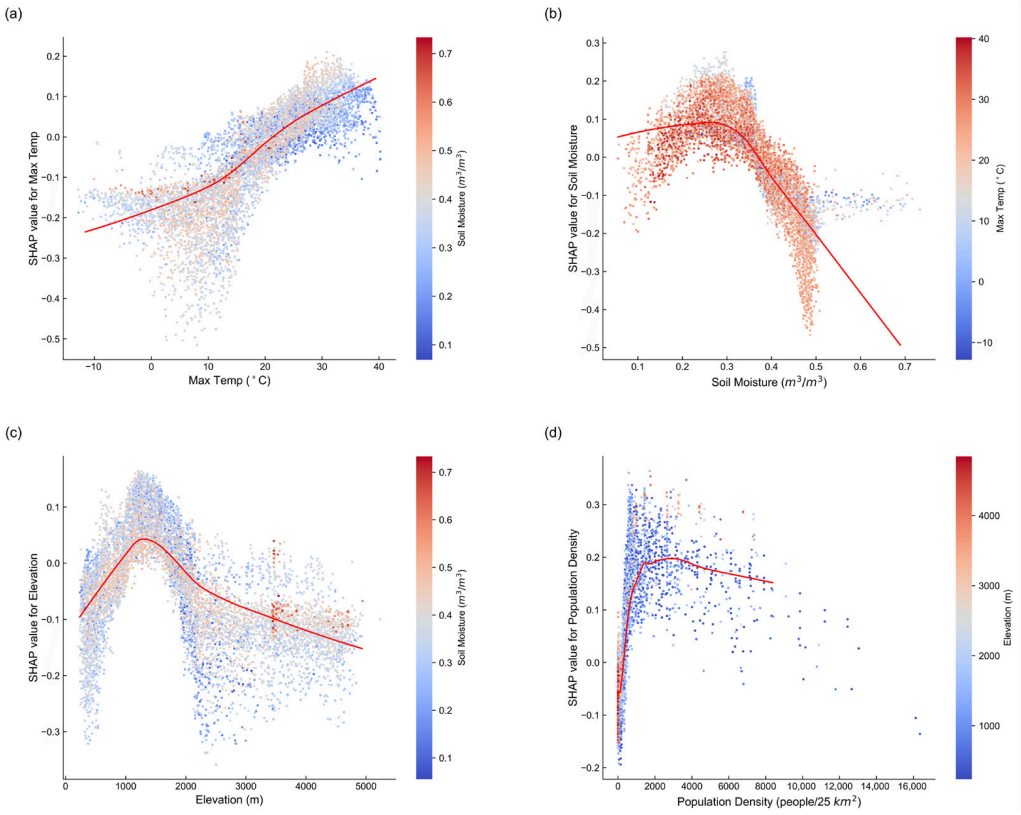


Figure 6. SHAP dependence plots of feature interactions: (**a**) maximum temperature and soil moisture; (**b**) soil moisture and maximum temperature; (**c**) elevation and soil moisture; (**d**) population density and elevation.

As shown in Figure 6c, in the low-to-mid altitude zones of 1000–2000 m, lower humidity readily created ranges associated with elevated susceptibility for fires, whereas in high-altitude areas, even if the environment was arid, fire susceptibility did not exhibit marked elevations. This elucidates that elevation can govern the response relationship between humidity and fire susceptibility by altering local hydrothermal conditions, reflecting an environment-constrained statistical interaction.

Figure 6d portrays the superimposed effects of population density and elevation. The fire-promoting role of human factors was principally concentrated in low-to-mid altitude zones; in high-altitude terrains exceeding 3000 m, the fire-promoting impacts of equivalent scales of population activity were significantly suppressed.

Coupled with the two-dimensional partial dependence plots (Figure 7), the statistical response ranges for fire susceptibility driving factors in Southwest China were further analyzed. The joint response surface (Figure 7a) suggests that higher model outputs were concentrated in a dry-hot statistical response range characterized by relatively high maximum temperature (above 25–30 °C) and low soil moisture (below 0.35 m^3/m^3). Under

low-temperature and high-humidity conditions, fire susceptibility established a range associated with reduced susceptibility (below roughly 0.20), signifying that moist and cold environments negatively associate with burning conditions. These values should be interpreted as statistical response ranges within the fitted model rather than as universal physical thresholds for fire occurrence.

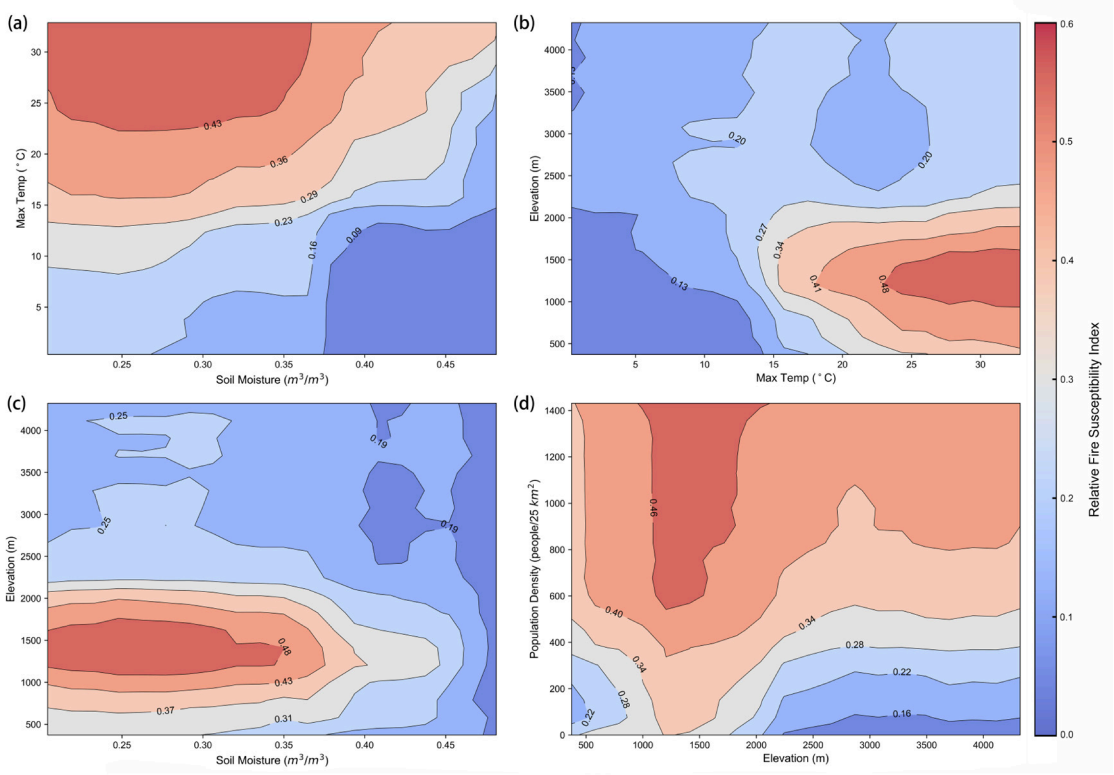


Figure 7. Two-dimensional partial dependence plots of key feature interactions: (**a**) soil moisture and the maximum temperature; (**b**) maximum temperature and elevation; (**c**) soil moisture and elevation; (**d**) elevation and population density.

Integrating Figure 7b–d, it becomes evident that elevation has distinct interactive response intervals with maximum temperature, soil moisture, and population density. Generally, elevation exerts a discernible attenuating effect on the driving roles of these meteorological and anthropogenic factors. The strong positive associations of high temperatures, droughts, and moderate human activities on fires were largely consolidated in low-altitude zones below 1500 m. Once elevation transcended 2500 m, even if the environment remained hot, dry, or subjected to human interference, fire susceptibility was significantly constrained (usually <0.30). This manifests that fire occurrence is associated with the superimposition of multi-dimensional factors; only when these factors collectively form high-response intervals do they constitute the core background conditions for fire occurrences in Southwest China.

Synthesizing the results from both types of plots, it is evident that fire susceptibility in the study area is not dominated by a single factor but rather exhibits multi-factor non-linear statistical interactions formed by the joint effects of meteorological factors, topographical factors, and human activities. The combined application of SHAP feature dependence plots and two-dimensional partial dependence plots qualitatively reveals the conditional dependence trends of fire-driving factors and quantitatively analyzes the statistical response ranges of composite fire-driving factors within the statistical model. This approach improves the statistical interpretability of the data-driven fire susceptibility assessment model to a certain extent.

4.5. Spatiotemporal Distribution Characteristics of Fire Susceptibility in Southwest China

The output results of the Random Forest model constructed in this study are relative fire susceptibility indices on a daily scale. To reveal the overall background pattern and seasonal differentiation characteristics of relative fire susceptibility indices in Southwest China from a macro-temporal scale, a "compute-then-aggregate" operational strategy was adopted. Specifically, the daily relative fire susceptibility indices during the 2019–2024 testing period were temporally aggregated by calculating the arithmetic mean for each 5 km grid cell. Subsequently, the Natural Breaks method was applied specifically to this pooled, multi-year averaged susceptibility layer to derive the global unified classification thresholds. This fixed statistical response threshold was partitioned into five tiers: Very Low, Low, Moderate, High, and Very High. Employing a globally fixed threshold is sufficiently motivated by the necessity to guarantee strict scale consistency and numerical comparability when calculating areal proportions and fire hit rates across disparate years.

According to the comparison results in Figure 8, the high fire susceptibility areas in the study region display prominent local clustering traits spatially, maintaining relatively steady spatial contours overall. However, influenced by interannual climate fluctuations, the boundaries of highly susceptible patches also experienced varying degrees of shrinkage and expansion each year. The orange and red patches representing high and very high susceptibility were predominantly located in central-southern Yunnan, southern Guizhou, and areas around the Hengduan Mountains. Sporadic high-susceptibility patches also existed along the fringes of the Sichuan Basin and in hilly terrains with relatively dense human activities and agriculture-forestry ecotones.

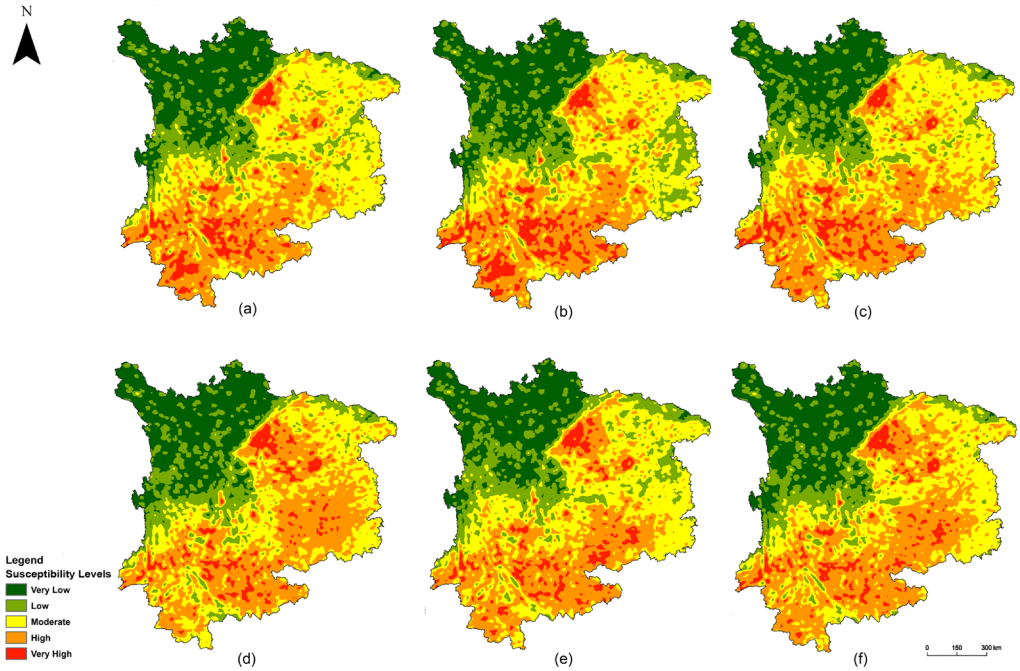


Figure 8. The background and pattern of susceptibility levels for fire hazards in the southwestern region from 2019 to 2024 (maps (**a**–**f**) represent the period from 2019 to 2024 respectively).

To test the classification efficacy of the model regarding fire susceptibility in Southwest China, this study conducted statistical validation on the spatial correspondence between actual fire points and susceptibility levels; the statistical findings are presented in Table 4.

Table 4. Annual proportions of regional area and actual fire occurrences relative to the total fire occurrences across detailed fire susceptibility levels from 2019 to 2024 (%).

Fire Susceptibility Class	Proportion (%)	2019	2020	2021	2022	2023	2024
Very Low	Fire Points	3.30	5.32	3.69	4.62	2.75	3.77
	Area	29.93	31.18	28.36	30.01	28.85	30.24
Low	Fire Points	8.57	10.74	8.41	13.41	10.28	8.32
	Area	22.20	22.50	19.17	21.27	24.14	19.16
Moderate	Fire Points	22.17	15.73	21.31	17.01	24.93	18.95
	Area	21.51	17.42	23.31	17.39	21.07	20.73
High	Fire Points	47.09	47.52	47.96	41.70	45.21	49.43
	Area	21.24	23.20	23.86	26.27	20.76	24.77
Very High	Fire Points	18.87	20.68	18.63	23.25	16.83	19.52
	Area	5.13	5.70	5.30	5.06	5.18	5.10

As detailed in Table 4, the model results exhibited consistent spatial matching features across the cross-year transferability dataset from 2019 to 2024. Higher fire susceptibility levels corresponded to larger proportions of actual fire points within smaller regional areas, while the reverse was true for lower susceptibility levels. As illustrated in Figure 9, the proportion of actual fire points falling within the High and Very High susceptibility levels ranged from 62.04% to 68.95%, whereas the corresponding regional area occupied by these two levels accounted for 25.94% to 31.33%. In contrast, the Low and Very Low susceptibility levels accounted for approximately 50% of the total regional area but contained less than 20% of the actual fire points. This difference in proportions indicates the RF model's capability to differentiate areas of higher fire susceptibility from the broader regional background, maintaining its spatial discriminative performance across years. Because the test period shares the same spatial domain as the training data, these results should be interpreted as evidence of cross-year transferability rather than full spatiotemporal independence.

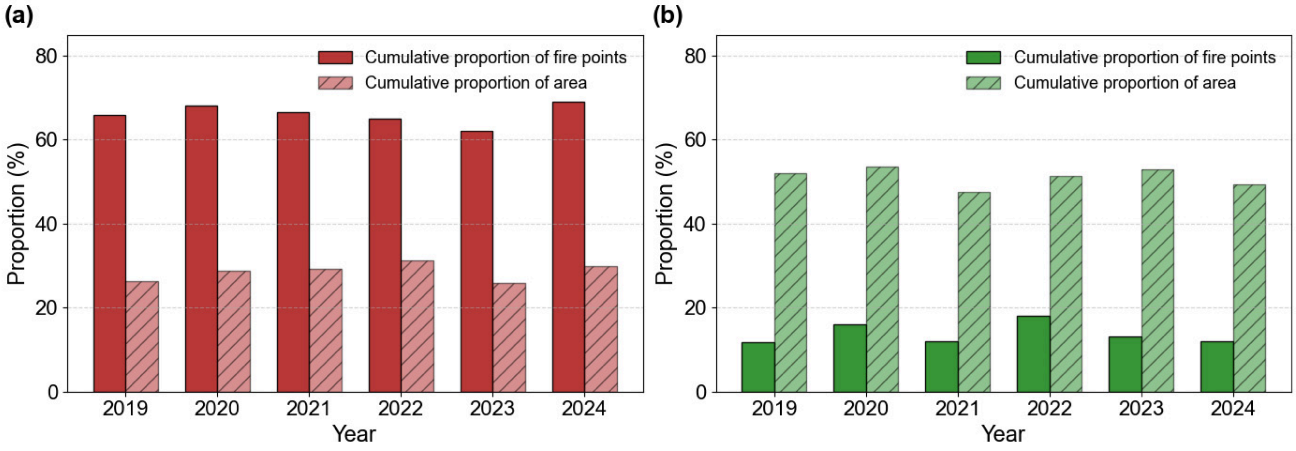


Figure 9. Histograms of regional area proportions and proportions of fire points within aggregated fire susceptibility levels from 2019 to 2024: (**a**) High susceptibility levels (High + Very High); (**b**) Low susceptibility levels (Low + Very Low).

Contrasting with the interannually stable susceptibility contours shown in Figure 8, the four-season fire susceptibility tier distributions illustrated in Figure 10 exhibited substantial differentiation. Seasonal results based on daily aggregation indicated that spring is the peak season for regional fires, with highly susceptible domains widely covering the core areas of central-southern Yunnan and southern Guizhou. During summer, influenced by the humidification of the Southwest Monsoon, the region's overall susceptibility levels

decreased significantly. Over the autumn and winter seasons, as precipitation dwindled and vegetation withered, the spatial proportion of high-susceptibility domains gradually surged once more, laying down the cumulative background for the spring's peak outbreaks.

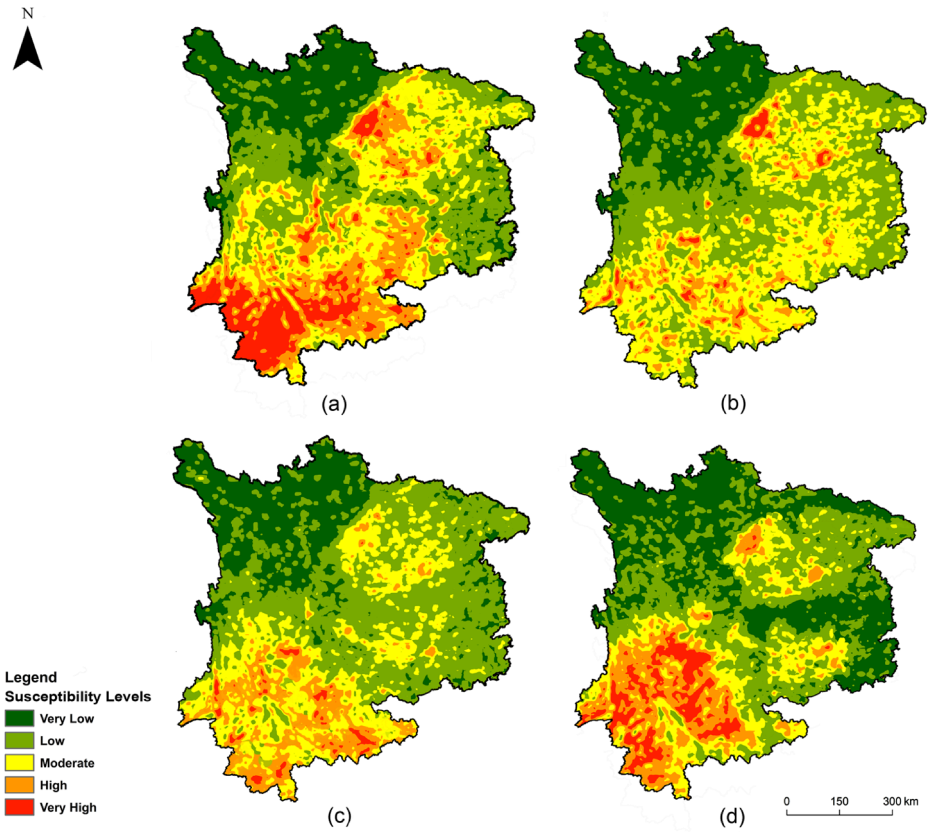


Figure 10. Four-season fire susceptibility background patterns in Southwest China from 2019 to 2024: (**a**) spring, (**b**) summer, (**c**) autumn, and (**d**) winter.

4.6. Spatial Autocorrelation and Cold/Hot Spot Clustering Features of Fire Susceptibility

Across multiple temporal scales, this study employed spatial statistical methods to systematically scrutinize the spatial structural attributes and temporal stability of fire susceptibility from 2019 to 2024. The interannual Global Moran's I indices, computed utilizing the Queen contiguity weight matrix, fluctuated around roughly 0.75 across the years (Figure 11). The mean Z-score was 330.10, which passed the statistical significance testing ($p < 0.01$, Z-score > 2.58). It should be clarified that while a Moran's I of ~0.75 indicates a relatively strong correlation rather than a perfect one, the unusually high Z-scores (e.g., ~330) are mathematically driven by the exceptionally large sample size (N) of the 5 km grid cells across the study area [49]. In spatial statistics, such a massive N dramatically reduces the variance, yielding extreme Z-scores that reflect absolute statistical confidence rather than an overestimation of the spatial correlation strength. This indicates that fire susceptibility consistently exhibits a significant positive spatial autocorrelation [50], with modest interannual variation magnitudes.

The spatial clustering patterns of cold and hot spots in the LISA local clustering outcomes (Figure 12) intuitively convey the macro-scale clustering distribution of fire susceptibility. Evaluating spatial association traits, the study region exhibited significant spatial heterogeneity and contiguous clustered patterns. In the low-altitude terrains of central-southern Yunnan and southern Guizhou, coupled with the dry-hot valley ecotones strongly affected by foehn effects around the Hengduan Mountains, large, continuous "High-High" significant clustering zones (i.e., hot spots) were observed. Conversely, the

majority of the Western Sichuan Plateau and high-elevation areas of northwestern Yunnan exhibited stable "Low-Low" significant clustering tracts (i.e., cold spots). Spatial outliers marked "High-Low" and "Low-High" constituted a minor proportion of the entire study area, distributed sporadically along abrupt elevational transition zones bordering hot and cold spots or within localized anomalous microclimates.

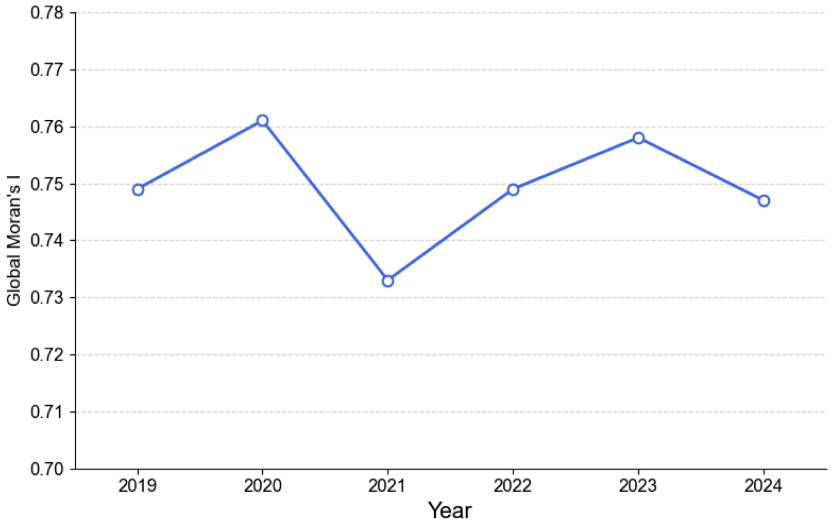


Figure 11. The inter-annual variation in the Moran's I index for fire susceptibility.

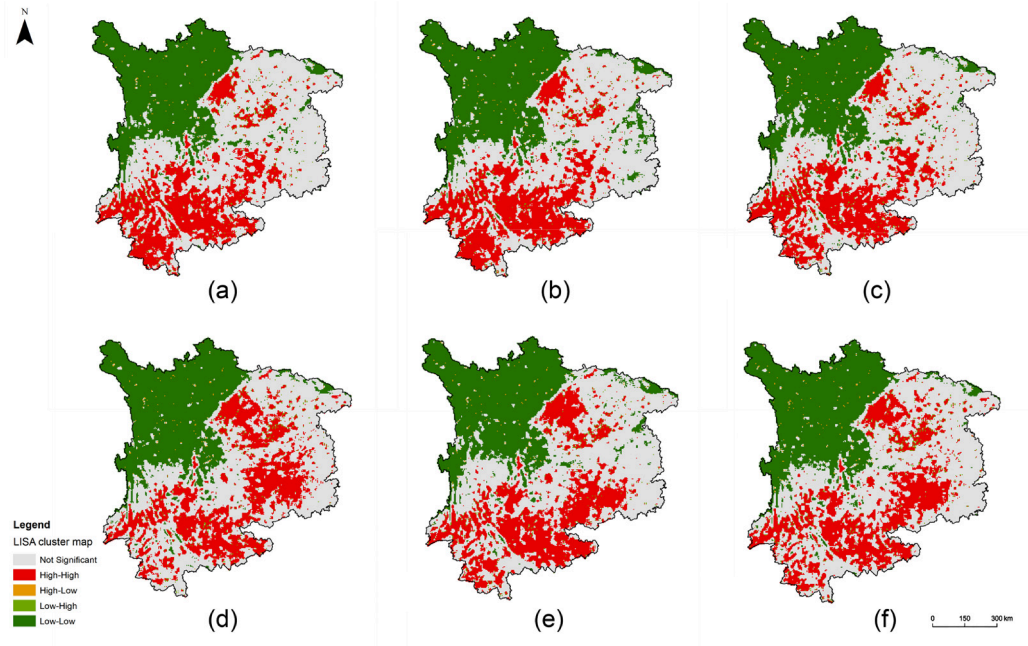


Figure 12. Cluster distribution of local spatial autocorrelation (LISA) of fire susceptibility in the southwestern region from 2019 to 2024 (maps (**a**–**f**) represent the period from 2019 to 2024 respectively).

In summary, spatial autocorrelation analysis was used to characterize the geographic organization of the susceptibility surface, rather than to provide an independent measure of prediction accuracy. The contiguously clustered hot and cold spots clearly define the geographical boundaries separating high and low susceptibilities. This phenomenon likely reflects the spatial continuity of underlying driving factors such as meteorology and topography, providing intuitive macro-scale pattern references for regional collaborative defense and control management.

5. Discussion

5.1. Sample Configuration Strategy and Model Applicability

Fire events exhibit extreme geographic sparsity. This study adopted a 1:2 positive-to-negative sample training strategy, which fundamentally represents a compromise between preserving the model's identification capability and maintaining class priors. As demonstrated in the multi-model sensitivity analysis, this configuration maintains a relatively high recall rate while avoiding extreme classification rigidity caused by severe class imbalance. Because negative under-sampling alters the class prior in the training set, the model output should not be interpreted as a calibrated probability. Model comparisons revealed that RF demonstrated superior overall performance with an AUC of 0.9167, as it is relatively effective at handling complex non-linear interactions among diverse environmental variables, and it maintained fire point capture rates of 62.04–68.95% within high-susceptibility districts. However, due to the inherent spatial dependence among the 5 km grid cells, these capture rates and the high AUC value may potentially be inflated in the absence of Spatial Block Cross-Validation. The independent test conducted using annual fire records from 2019 to 2024 indicates that the model exhibits relatively stable cross-year transferability within the study domain. Because the cross-year transferability test still shares the same spatial extent as the training data, these results should not be interpreted as strict spatiotemporal dual-independent generalization capabilities.

5.2. Statistical Response of Key Fire-Driving Factors

Soil moisture, maximum temperature, elevation, and population density are the key fire-driving factors associated with changes in fire susceptibility across Southwest China. The combined analysis of SHAP and PDP results indicates that fire susceptibility in the study area exhibits significant non-linear responses to wet-dry conditions, thermal environments, topographic backgrounds, and proxy variables for human activities. Among these factors, the combination of low soil moisture and higher maximum temperatures corresponds to higher model outputs, indicating that it is statistically associated with elevated regional fire susceptibility. Daily soil moisture practically reflects the long-term results of the interaction between precipitation and evaporation to a certain extent; its deficit severity signals a continuous decline in fuel moisture content, exhibiting pronounced cumulative proxy attributes. NDVI similarly maps the cumulative state of vegetation biomass. Intermediate elevation ranges show relatively higher susceptibility levels, whereas lower and higher elevations generally correspond to reduced model outputs. This pattern likely reflects the combined effects of vegetation distribution, climate gradients, and human activity intensity along elevation gradients. Moderate population densities are associated with increased susceptibility, whereas very high-density areas show a declining trend in susceptibility, which may reflect intensive land development and more effective fire prevention and suppression activities. When proxy variables such as population density and elevation are involved, the model's non-linear responses across different intervals are likely co-moderated by unobserved confounding factors (such as land-use patterns, vegetation types, and the intensity of anthropogenic fire suppression).

Although the model somewhat reflects the statistical convergence characteristics of long-term cumulative environmental stress and concurrent instantaneous triggers (e.g., maximum temperature), the fire susceptibility assessment model developed in this study performs a concurrent diagnosis rather than traditional future-tense forecasting. It evaluates the relative fire susceptibility driven strictly by same-day environmental backgrounds, and its statistical outputs substantively reveal the non-linear response characteristics of fire-driving factors rather than strictly proven causal mechanisms.

5.3. Spatial Clustering Characteristics of Fire Susceptibility

Global Moran's I confirms that the model-identified fire susceptibility exhibits significant positive spatial autocorrelation, indicating a non-random spatial distribution. LISA analysis further reveals distinct "hot and cold spot" patterns. These local clusters delineate the spatial organization of fire susceptibility, identifying regions where adjacent grids exhibit similarly high or low susceptibility levels. It must be emphasized that Moran's I and LISA are employed solely to characterize the spatial organizational structure of susceptibility, rather than to validate model performance. These spatial clustering insights provide a critical geographical reference for cross-jurisdictional joint fire defense and resource allocation. Specifically, the delineation of local hotspots can assist decision-makers in prioritizing fire monitoring, fuel management, and emergency preparedness at a broader management scale.

5.4. Future Research Prospects

This study has made certain progress concerning macro-scale fire susceptibility assessment and the statistical attribution of key drivers. Nonetheless, there is still room for further improvement regarding data representation, methodology, and analytical interpretation.

Conceptually, because the daily explanatory variables were aligned with fire labels on the same day, the framework functions as a concurrent susceptibility diagnosis rather than strict forward-looking forecasting, and it does not discern the causal directionality between influencing factors and fire occurrence within micro-scale contexts. Furthermore, although the LOCF method preserves strict temporal causality for dynamic spatiotemporal matching, it may introduce localized step-like discontinuities during periods of rapid phenological transition, potentially reducing the temporal smoothness of seasonal vegetation dynamics. Consequently, the response ranges identified by SHAP and PDP should be interpreted as model-based statistical patterns rather than causal mechanisms or universal physical thresholds. To mitigate the potential reverse causality inherent in same-day matching and the interpretive ambiguity arising from the integration of temporally asynchronous variables, future studies should incorporate time-lagged predictive features alongside explicit long-term stress indicators (e.g., standardized drought indices). Such an approach would help disentangle the effects of antecedent cumulative environmental stress from those of immediate meteorological triggers, thereby reducing temporal confounding and enhancing the interpretability of fire-driver relationships.

From a spatial and data resolution perspective, a 5 km grid facilitates the unification of multi-source inputs, yet concurrently reduces the representational accuracy of micro-topography, micro-scale wind vectors, and variations in localized human activities [51]. Restricted by sensor resolution constraints, it is also difficult to completely avoid omission and commission errors with MODIS active fire products. Additionally, anthropogenic factors like population density and road grids function primarily as long-term background proxy factors in this paper, which is insufficient to capture short-term, dynamic disturbances like sporadic agricultural burns. In the future, integrating higher-resolution fire point datasets, dynamic land-use maps, and near-real-time human activity data holds merit for improving the accuracy of sample labeling and driving variables [52,53].

Methodologically, the current framework entails certain structural uncertainties in variable representation and feature selection. First, although the scalar transformation of aspect and wind direction reflects general solar radiation contrasts, condensing circular orientations into a single scalar in highly heterogeneous terrains inevitably results in the loss of fine-grained directional components. This heuristic encoding inherently restricts the model's behavior, and the interpretability of this feature is strictly confined to its role as a proxy for hydrothermal exposure rather than a comprehensive representation of true

geographic orientation. Accordingly, the SHAP and PDP outputs associated with aspect and wind direction should be interpreted as statistical responses to the encoded hydrothermal exposure gradient rather than as complete representations of true directional effects. Second, while VIF filtering was deliberately utilized to prevent interpretation distortion in SHAP and PDP analyses, its strict applicability as a selection criterion in non-linear modeling contexts warrants further methodological scrutiny. Moreover, these structural choices interact with underlying sample distributions to jointly shape the observed response curves, which should not be interpreted as purely reflecting objective environmental mechanisms. To address these uncertainties, subsequent efforts will comparatively evaluate multi-dimensional encoding schemes (e.g., dual sin/cos vector transformations) to achieve a more comprehensive representation of micro-environmental drivers and simultaneously investigate the impacts on explanation robustness when highly collinear variables (such as mean and maximum temperatures) are retained.

Furthermore, regarding validation and sample design, the stratified cross-validation deployed herein primarily serves the preliminary comparison of baseline algorithms. Affected by residual spatiotemporal dependence among samples, these metrics might yield overly optimistic results. Although subsequent time-extrapolation tests partially address this issue, such dependencies remain a structural constraint. To strictly decouple spatial dependence and independently evaluate the model's practical application capability in unseen spatiotemporal environments, advanced protocols such as spatial block cross-validation and temporal blocking will be implemented. During the construction of negative samples, preliminary spatiotemporal screening rules should also be applied—excluding records from time windows immediately before and after fire events, as well as omitting adjacent grids surrounding fire locations on the ignition day—to further enhance methodological rigor.

Ultimately, integrating this data-driven model with mechanistic fire behavior process models, comprehensive ecogeographical analyses, and prolonged observational archives will be essential to cross-validate key response intervals and interaction relationships. Lastly, as this study focuses on evaluating the relative susceptibility governing fire ignitions, it has not yet incorporated exposure, vulnerability, and prevention/control capacities. If future research integrates information on population, infrastructure, ecological vulnerability, and fire suppression resources, the study could be extended from a single susceptibility analysis to a comprehensive regional risk assessment, which would ultimately enhance the application value of the research findings in early warning support and zoned governance [54].

6. Conclusions

This study developed a fire susceptibility assessment framework for Southwest China by integrating imbalanced sampling, machine-learning-based discrimination, and explainable analysis. Compared with LR and SVM, RF showed stronger discrimination performance on the available samples and produced a relatively stable spatial pattern of fire susceptibility tiers across different years within the same study region.

The interpretability analysis indicates that maximum temperature, soil moisture, elevation, and population density were key predictors in the fitted model. Their response patterns suggest that elevated susceptibility tended to occur under relatively dry and warm conditions, especially in low- to mid-elevation areas. These findings should be interpreted as statistical attribution results derived from the fitted model rather than as direct evidence of underlying physical causal mechanisms.

Overall, the proposed framework is suitable for macro-scale fire susceptibility assessment and spatial prioritization under observed environmental conditions, but further work is still needed on spatially independent validation, lagged predictor design, and probability calibration before it can be extended to strict forecasting applications.

Author Contributions: Conceptualization, J.L.; methodology, J.L.; software, J.L.; validation, J.L., X.G. and J.G.; formal analysis, F.D.; investigation, H.L.; resources, J.L.; data curation, Y.Z.; writing—original draft preparation, J.L.; writing—review and editing, F.D.; visualization, J.L.; supervision, H.L.; project administration, F.D. All authors have read and agreed to the published version of the manuscript.

Funding: This research received no specific grant from any funding agency in the public, commercial, or not-for-profit sectors. The authors have no acknowledgments to report.

Institutional Review Board Statement: Not applicable.

Informed Consent Statement: Not applicable.

Data Availability Statement: All data and materials are available on request from the corresponding author. The data are not publicly available due to ongoing research using a part of the data.

Conflicts of Interest: The authors declare no conflicts of interest.

References

1. Jones, M.W.; Abatzoglou, J.T.; Veraverbeke, S.; Andela, N.; Lasslop, G.; Forkel, M.; Smith, A.J.P.; Burton, C.; Betts, R.A.; Van Der Werf, G.R.; et al. Global and Regional Trends and Drivers of Fire Under Climate Change. *Rev. Geophys.* **2022**, *60*, e2020RG000726. [CrossRef]
2. Hardy, C.C. Wildland Fire Hazard and Risk: Problems, Definitions, and Context. *For. Ecol. Manag.* **2005**, *211*, 73–82. [CrossRef]
3. Bowman, D.M.J.S.; Williamson, G.J.; Abatzoglou, J.T.; Kolden, C.A.; Cochrane, M.A.; Smith, A.M.S. Human Exposure and Sensitivity to Globally Extreme Wildfire Events. *Nat. Ecol. Evol.* **2017**, *1*, 0058. [CrossRef] [PubMed]
4. Afrin, S.; Garcia-Menendez, F. Potential Impacts of Prescribed Fire Smoke on Public Health and Socially Vulnerable Populations in a Southeastern U.S. State. *Sci. Total Environ.* **2021**, *794*, 148712. [CrossRef] [PubMed]
5. Xing, H.; Fang, K.; Yao, Q.; Zhou, F.; Ou, T.; Liu, J.; Zhou, S.; Jiang, S.; Chen, Y.; Bai, M.; et al. Impacts of Changes in Climate Extremes on Wildfire Occurrences in China. *Ecol. Indic.* **2023**, *157*, 111288. [CrossRef]
6. Li, X.; Liu, X.; Zhang, H.; Bao, W. Latitudinal Patterns of Climatic Variables and Influence of Local Topography on Climatic Variables in the Dry Valleys of Southwestern China. *J. Mt. Sci.* **2022**, *19*, 1348–1356. [CrossRef]
7. Cui, L.; Luo, C.; Yao, C.; Zou, Z.; Wu, G.; Li, Q.; Wang, X. The Influence of Climate Change on Forest Fires in Yunnan Province, Southwest China Detected by GRACE Satellites. *Remote Sens.* **2022**, *14*, 712. [CrossRef]
8. Zhang, X.; Fan, J.; Zhou, J.; Gui, L.; Bi, Y. Mapping fire severity in Southwest China using the combination of Sentinel 2 and GF series satellite images. *Sensors* **2023**, *23*, 2492. [CrossRef] [PubMed]
9. Phelps, N.; Woolford, D.G. Comparing Calibrated Statistical and Machine Learning Methods for Wildland Fire Occurrence Prediction: A Case Study of Human-Caused Fires in Lac La Biche, Alberta, Canada. *Int. J. Wildland Fire* **2021**, *30*, 850–870. [CrossRef]
10. Chang, Y.; Zhu, Z.; Bu, R.; Chen, H.; Feng, Y.; Li, Y.; Hu, Y.; Wang, Z. Predicting Fire Occurrence Patterns with Logistic Regression in Heilongjiang Province, China. *Landsc. Ecol.* **2013**, *28*, 1989–2004. [CrossRef]
11. Ma, W.; Feng, Z.; Cheng, Z.; Chen, S.; Wang, F. Identifying Forest Fire Driving Factors and Related Impacts in China Using Random Forest Algorithm. *Forests* **2020**, *11*, 507. [CrossRef]
12. Guo, F.; Wang, G.; Su, Z.; Liang, H.; Wang, W.; Lin, F.; Liu, A. What Drives Forest Fire in Fujian, China Evidence from Logistic Regression and Random Forests. *Int. J. Wildland Fire* **2016**, *25*, 505–519. [CrossRef]
13. Lau, C.K.; Lai, K.K.; Lee, Y.P.; Du, J. Fire risk assessment with scoring system, using the support vector machine approach. *Fire Saf. J.* **2015**, *78*, 188–195. [CrossRef]
14. Gigović, L.; Pourghasemi, H.R.; Drobnjak, S.; Bai, S. Testing a New Ensemble Model Based on SVM and Random Forest in Forest Fire Susceptibility Assessment and Its Mapping in Serbia's Tara National Park. *Forests* **2019**, *10*, 408. [CrossRef]
15. Rudin, C. Why Black Box Machine Learning Should Be Avoided for High-Stakes Decisions, in Brief. *Nat. Rev. Methods Primers* **2022**, *2*, 81. [CrossRef]
16. Chaparro, D.; Vall-llossera, M.; Piles, M.; Camps, A.; Rüdiger, C.; Riera-Tatché, R. Predicting the Extent of Wildfires Using Remotely Sensed Soil Moisture and Temperature Trends. *IEEE J. Sel. Top. Appl. Earth Obs. Remote Sens.* **2016**, *9*, 2818–2829. [CrossRef]
17. Quan, X.; Jiao, M.; He, Z.; Jaafari, A.; Xie, Q.; Lai, X. Effects of different sampling strategies for unburned label selection in machine learning modelling of wildfire occurrence probability. *Int. J. Wildland Fire* **2023**, *32*, 561–575. [CrossRef]
18. Shao, Y.; Zhu, Q.; Feng, Z.; Sun, L.; Yue, P.; Wang, A.; Zhang, X.; Su, Z. Utilizing Grid Data and Deep Learning for Forest Fire Occurrences and Decision Support: A Case Study in the Ningxia Hui Autonomous Region. *Forests* **2023**, *14*, 2418. [CrossRef]

19. Zhang, Y.; Huang, Z.; Tian, Y.; Lin, J.; Qin, C. Time-lag and cumulative effects of extreme climate on vegetation coverage change in Southwest China. *Ecol. Environ. Sci.* **2025**, *34*, 665–677. (In Chinese) [CrossRef]
20. Pang, Y.; Zhou, C.; Wang, S.; Luo, Y. Climatic background analysis of anomalous cold-wet/warm-dry winters in Southwest China. *Acta Meteorol. Sin.* **2024**, *82*, 459–475. (In Chinese)
21. Hou, B.; Li, Q.; Yang, Y.; Zhang, L. Dynamic changes of forest fires with topographic factors in Southwest China from 2003 to 2020 based on MODIS data. *Ecol. Sci.* **2024**, *43*, 131–137. (In Chinese) [CrossRef]
22. Velastegui-Montoya, A.; Montalván-Burbano, N.; Carrión-Mero, P.; Rivera-Torres, H.; Sadeck, L.; Adami, M. Google Earth Engine: A Global Analysis and Future Trends. *Remote Sens.* **2023**, *15*, 3675. [CrossRef]
23. Gorelick, N.; Hancher, M.; Dixon, M.; Ilyushchenko, S.; Thau, D.; Moore, R. Google Earth Engine: Planetary-scale geospatial analysis for everyone. *Remote Sens. Environ.* **2017**, *202*, 18–27. [CrossRef]
24. Kaufman, S.; Rosset, S.; Perlich, C.; Stitelman, O. Leakage in data mining: Formulation, detection, and avoidance. *ACM Trans. Knowl. Discov. Data* **2012**, *6*, 1–21. [CrossRef]
25. Beers, T.W.; Dress, P.E.; Wensel, L.C. Aspect transformation in site productivity research. *J. For.* **1966**, *64*, 691–692. [CrossRef]
26. Molnar, C. *Interpretable Machine Learning: A Guide for Making Black Box Models Explainable*, 2nd ed.; Shroff: Maharashtra, India, 2022. Available online: https://christophm.github.io/interpretable-ml-book/ (accessed on 7 March 2026).
27. Aas, K.; Jullum, M.; Løland, A. Explaining individual predictions when features are dependent: More accurate approximations to Shapley values. *Artif. Intell.* **2021**, *298*, 103502. [CrossRef]
28. Abatzoglou, J.T.; Williams, A.P. Impact of anthropogenic climate change on wildfire across western US forests. *Proc. Natl. Acad. Sci. USA* **2016**, *113*, 11770–11775. [CrossRef] [PubMed]
29. Kondylatos, S.; Prapas, I.; Camps-Valls, G.; Papoutsis, I. Mesogeos: A multi-purpose dataset for data-driven wildfire modeling in the Mediterranean. *Adv. Neural Inf. Process. Syst.* **2023**, *36*, 50661–50676. [CrossRef]
30. Kondylatos, S.; Prapas, I.; Ronco, M.; Papoutsis, I.; Camps-Valls, G.; Piles, M. Wildfire danger prediction and understanding with deep learning. *Geophys. Res. Lett.* **2022**, *49*, e2022GL099368. [CrossRef]
31. Gao, C.; Lin, H.; Hu, H. Forest-Fire-Risk Prediction Based on Random Forest and Backpropagation Neural Network of Heihe Area in Heilongjiang Province, China. *Forests* **2023**, *14*, 170. [CrossRef]
32. Huang, P.; Peng, L.; Pan, H. Linking the Random Forests Model and GIS to Assess Geo-Hazards Risk: A Case Study in Shifang County, China. *IEEE Access* **2020**, *8*, 28033–28042. [CrossRef]
33. Biau, G. Analysis of a random forests model. *J. Mach. Learn. Res.* **2012**, *13*, 1063–1095.
34. Breiman, L. Random Forests. *Mach. Learn.* **2001**, *45*, 5–32. [CrossRef]
35. Shao, Y.; Feng, Z.; Sun, L.; Yang, X.; Li, Y.; Xu, B.; Chen, Y. Mapping China's Forest Fire Risks with Machine Learning. *Forests* **2022**, *13*, 856. [CrossRef]
36. LaValley, M.P. Logistic Regression. *Circulation* **2008**, *117*, 2395–2399. [CrossRef] [PubMed]
37. Guo, F.; Zhang, L.; Jin, S.; Tigabu, M.; Su, Z.; Wang, W. Modeling Anthropogenic Fire Occurrence in the Boreal Forest of China Using Logistic Regression and Random Forests. *Forests* **2016**, *7*, 250. [CrossRef]
38. Hearst, M.A.; Dumais, S.T.; Osuna, E.; Platt, J.; Scholkopf, B. Support vector machines. *IEEE Intell. Syst. Their Appl.* **1998**, *13*, 18–28. [CrossRef]
39. Li, Y.; Feng, Z.; Chen, S.; Zhao, Z.; Wang, F. Application of the Artificial Neural Network and Support Vector Machines in Forest Fire Prediction in the Guangxi Autonomous Region, China. *Discret. Dyn. Nat. Soc.* **2020**, *2020*, 5612650. [CrossRef]
40. Liao, L.; Zhu, X. Predicting Wildfire Risk in Southwestern Saudi Arabia Using Machine Learning and Geospatial Analysis. *Remote Sens.* **2025**, *17*, 3516. [CrossRef]
41. Carrington, A.M.; Manuel, D.G.; Fieguth, P.W.; Ramsay, T.; Osmani, V.; Wernly, B.; Bennett, C.; Hawken, S.; Magwood, O.; Sheikh, Y.; et al. Deep ROC Analysis and AUC as Balanced Average Accuracy, for Improved Classifier Selection, Audit and Explanation. *IEEE Trans. Pattern Anal. Mach. Intell.* **2023**, *45*, 329–341. [CrossRef] [PubMed]
42. Erbani, J.; Portier, P.-É.; Egyed-Zsigmond, E.; Nurbakova, D. Confusion Matrices: A Unified Theory. *IEEE Access* **2024**, *12*, 181372–181419. [CrossRef]
43. Seo, M.; Castillo-Osorio, E.; Yoo, H. Fire Risk Prediction Analysis Using Machine Learning Techniques. *Sens. Mater.* **2023**, *35*, 3241. [CrossRef]
44. Wang, H.; Liang, Q.; Hancock, J.T.; Khoshgoftaar, T.M. Feature Selection Strategies: A Comparative Analysis of SHAP-Value and Importance-Based Methods. *J. Big Data* **2024**, *11*, 44. [CrossRef]
45. Lundberg, S.M.; Lee, S.-I. A Unified Approach to Interpreting Model Predictions. In *Proceedings of the Advances in Neural Information Processing Systems*; Curran Associates, Inc.: Red Hook, NY, USA, 2017; Volume 30, pp. 4765–4774.
46. Kerrigan, D.; Barr, B.; Bertini, E. PDPilot: Exploring Partial Dependence Plots Through Ranking, Filtering, and Clustering. *IEEE Trans. Vis. Comput. Graph.* **2025**, *31*, 7377–7390. [CrossRef] [PubMed]
47. You, W.; Lin, L.; Wu, L.; Ji, Z.; Yu, J.; Zhu, J.; Fan, Y.; He, D. Geographical Information System-Based Forest Fire Risk Assessment Integrating National Forest Inventory Data and Analysis of Its Spatiotemporal Variability. *Ecol. Indic.* **2017**, *77*, 176–184. [CrossRef]

48. Su, Z.; Tigabu, M.; Cao, Q.; Wang, G.; Hu, H.; Guo, F. Comparative analysis of spatial variation in forest fire drivers between boreal and subtropical ecosystems in China. *For. Ecol. Manag.* **2019**, *454*, 117669. [CrossRef]
49. Anselin, L.; Lin, M.; Lucas, H.C., Jr.; Shmueli, G. Research commentary—Too big to fail: Large samples and the p-value problem. *Inf. Syst. Res.* **2013**, *24*, 906–917.
50. Anselin, L. Local Indicators of Spatial Association—LISA. *Geogr. Anal.* **1995**, *27*, 93–115. [CrossRef]
51. Li, W.; Xu, Q.; Yi, J.; Liu, J. Predictive Model of Spatial Scale of Forest Fire Driving Factors: A Case Study of Yunnan Province, China. *Sci. Rep.* **2022**, *12*, 19029. [CrossRef] [PubMed]
52. Bakke, S.J.; Wanders, N.; van der Wiel, K.; Tallaksen, L.M. A Data-Driven Model for Fennoscandian Wildfire Danger. *Nat. Hazards Earth Syst. Sci.* **2023**, *23*, 65–89. [CrossRef]
53. Reichstein, M.; Camps-Valls, G.; Stevens, B.; Jung, M.; Denzler, J.; Carvalhais, N.; Prabhat, F. Deep Learning and Process Understanding for Data-Driven Earth System Science. *Nature* **2019**, *566*, 195–204. [CrossRef] [PubMed]
54. Yue, W.; Ren, C.; Liang, Y.; Liang, J.; Lin, X.; Yin, A.; Wei, Z. Assessment of Wildfire Susceptibility and Wildfire Threats to Ecological Environment and Urban Development Based on GIS and Multi-Source Data: A Case Study of Guilin, China. *Remote Sens.* **2023**, *15*, 2659. [CrossRef]

Disclaimer/Publisher's Note: The statements, opinions and data contained in all publications are solely those of the individual author(s) and contributor(s) and not of MDPI and/or the editor(s). MDPI and/or the editor(s) disclaim responsibility for any injury to people or property resulting from any ideas, methods, instructions or products referred to in the content.